JACS
JOURNAL OF THE AMERICAN CHEMICAL SOCIETY
Communication
pubs.acs.org/JACS

Liquid-Based Growth of Polymeric Carbon Nitride Layers and Their Use in a Mesostructured Polymer Solar Cell with V_{oc} Exceeding 1 V

Jingsan Xu,[†] Thomas J. K. Brenner,*[,‡] Laurent Chabanne,[†] Dieter Neher,[‡] Markus Antonietti,[†] and Menny Shalom*[,†]

[†]Department of Colloid Chemistry, Max Planck Institute of Colloids and Interfaces, 14424 Potsdam, Germany
[‡]Institute of Physics & Astronomy, University of Potsdam, 14476 Potsdam, Germany

Supporting Information

ABSTRACT: Herein we report a general liquid-mediated pathway for the growth of continuous polymeric carbon nitride (C_3N_4) thin films. The deposition method consists of the use of supramolecular complexes that transform to the liquid state before direct thermal condensation into C_3N_4 solid films. The resulting films exhibit continuous porous C_3N_4 networks on various substrates. Moreover, the optical absorption can be easily tuned to cover the solar spectrum by the insertion of an additional molecule into the starting complex. The strength of the deposition method is demonstrated by the use of the C_3N_4 layer as the electron acceptor in a polymer solar cell that exhibits a remarkable open-circuit voltage exceeding 1 V. The easy, safe, and direct synthesis of carbon nitride in a continuous layered architecture on different functional substrates opens new possibilities for the fabrication of many energy-related devices.

In the last years, polymeric or graphitic carbon nitride (simplified as C_3N_4) has been widely used as a metal-free semiconductor catalyst for many energy-related applications.[1,2] Combining its stability at high temperatures (up to 600 °C in air) and in corrosive chemical environments, C_3N_4 shows good performance as a photocatalyst[3] (i.e., for water splitting, degradation of pollutants, etc.), an electrocatalyst,[4,5] and in heterogeneous catalysis.[6] Generally, the synthesis of bulk C_3N_4 involves thermal condensation of nitrogen- and carbon-rich monomers such as cyanamide, dicyanamide, and melamine.[1] This polymerization method is very simple and straightforward and is widely used for the preparation of C_3N_4 materials. A variety of approaches have been used to modify the chemical, optical, and electronic properties of C_3N_4 catalysts by metal[7] or nonmetal[8,9] doping, introduction of pores by templating methods,[10,11] formation of composites,[12−14] and precursor preorganization[15,16] or copolymerization.[17] Nevertheless, most of the modifications of C_3N_4 afford powders, while for (photo)electrochemical applications (i.e., water electrosplitting, fuel cells, and solar cells) a direct and continuous C_3N_4 layer is preferred.[8,18] Because of the large particle size of C_3N_4 along with its insolubility in most solvents, the common deposition methods (spin coating and screen printing) result in poor C_3N_4 coverage and weak adhesion on commonly used substrates (e.g., conductive transparent oxides such as FTO and ITO). Consequently, the C_3N_4 films usually exhibit low conductivity and demonstrate unsatisfying activity in electrical measurements.

Several attempts have been made to improve the performance of C_3N_4 in (photo)electrical devices. Schedel and co-workers heated dicyanamide in situ on a $CuGaS_2$ thin-film substrate for C_3N_4 growth, and the $CuGaS_2/C_3N_4$ composite showed light-induced H_2 evolution under bias.[19] In addition, the insertion of carbon nitride into highly ordered porous carbon or into graphene-based mesoporous silica was recently presented.[20,21] Very lately, our group used the cyanuric acid−melamine supramolecular complex (CM) to grow C_3N_4 films directly on FTO or TiO_2 and ZnO nanoparticle layers and demonstrated their activities over electrochemical H_2 evolution reactions.[22] However, this approach results in only a rather thin C_3N_4 layer (~40 nm) on FTO, which is not sufficient to act as the active layer for photoelectrochemical cells or photovoltaics because of the low light absorption. Moreover, the thickness and homogeneity of C_3N_4 films prepared by solid-state deposition are strongly dependent on the surface properties. In view of such conditions, alternative pathways for C_3N_4 film growth are of great interest.

Herein we report a liquid-based reaction for the growth of C_3N_4 thin films using the supramolecular approach on various substrates, including commercial FTO, metal foil, and ultrathin TiO_2 layers. Moreover, we also demonstrate the ability to tune the optical absorption of the deposited C_3N_4 by inserting barbituric acid (BA) as a dopant. The morphology and structure of the C_3N_4 films have been characterized by scanning electron microscopy (SEM), transmission electron microscopy (TEM), X-ray diffraction (XRD) and Fourier transform IR spectroscopy (FTIR), and the growth mechanism is discussed in detail. The strength of this deposition technique is demonstrated, as a proof of concept, by the fabrication of a photoactive electron acceptor layer of C_3N_4 in an organic solar cell.

The thin-film preparation process is schematically shown in Figure 1. Briefly, the CMp complex was prepared according to our previous report[16] simply by shaking a 1:1 (mol/mol) mixture of cyanuric acid (C) and 2,4-diamino-6-phenyl-1,3,5-triazine (Mp) in water. An adequate amount of dried CMp powder was transferred to a crucible, totally covering the substrate placed at the bottom. The crucible was then capped and heated at 550 °C for 4 h in a nitrogen atmosphere.

Received: May 22, 2014
Published: September 17, 2014

dx.doi.org/10.1021/ja508329c | J. Am. Chem. Soc. 2014, 136, 13486−13489

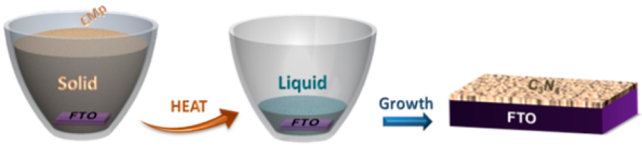

Figure 1. Schematic illustration of the process for preparing C_3N_4 films, with FTO as an example substrate.

Figure 2 shows SEM images of C_3N_4 grown on different substrates, including a thin TiO_2 layer (40 nm), molybdenum

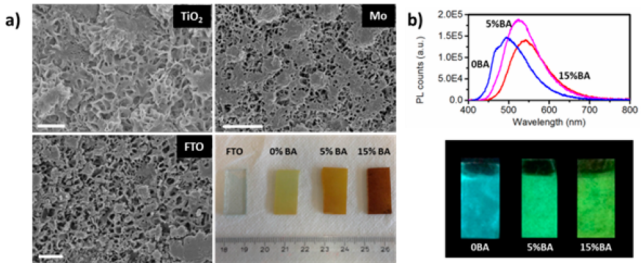

Figure 2. (a) Top-view SEM images of C_3N_4 film on different substrates: thin TiO_2 layer, Mo foil, and FTO glass. All scale bars are 2 μm. At the bottom right is a photograph of bare FTO and FTO with C_3N_4 films modified using different amounts of BA. (b) PL spectra of BA-modified C_3N_4 films on FTO and a photograph of the films under 365 nm illumination.

(Mo) foil, and FTO glass. In all cases, continuous C_3N_4 films were obtained, demonstrating complete coverage across the substrate. It is very interesting that all of the C_3N_4 films showed an ordered porous network morphology, since no template was used during the synthesis. This speaks for shrinkage in the last steps of material condensation organization (i.e., the material turns solid before final arrangements). Nevertheless, the whole film is built up by continuous and rather organized C_3N_4 strands. The resulting thickness of the C_3N_4 on thin TiO_2 substrate was ~500 nm, while the film grown on FTO was much thicker (>10 μm), probably because of the difference in surface wettability. It is important to note that the C_3N_4 films were strongly bound to the substrates, and sonication in water for 1 h was not able to peel them off.

The structure and composition of the films were further investigated by TEM, XRD, FTIR, and elemental analysis (EA). In order to carry out these measurements, powders were scratched from the substrates using a sharp blade. A TEM image of the TiO_2/C_3N_4 system (Figure S1a in the Supporting Information) indicates that TiO_2 nanoparticles (~70 nm) and sheetlike C_3N_4 integrate with each other very well. Another proof of the presence of C_3N_4 is given by the XRD pattern (Figure S1c), which shows the typical strong layered stacking peak of graphitic C_3N_4 at around 27.7°. In addition to XRD, the FTIR spectrum (Figure S1d) further confirms the formation of C_3N_4. Strong absorption bands located at 1200−1600 cm^{-1}, which are typical stretching modes of C_3N_4 heterocycles, alongside the characteristic vibration peak of triazine units at ~810 cm^{-1} are shown in FTIR spectra.[23] Besides, the optical absorption spectrum (Figure S1b) of the C_3N_4 film on TiO_2 shows an absorption edge at around 470 nm. Similar results were obtained for C_3N_4 on Mo and FTO (Figures S2 and S3). More evidence for the formation of carbon nitride is given by the EA data for C_3N_4 on FTO (Table S1). The C/N molar ratio is less than 1, meaning that on average only one phenyl group is present for three melem units.[16] The small amount of carbon in C_3N_4 compared with the CMp starting material indicates that during the reaction most of the phenyl groups evaporate (see below). In addition, the low amount of hydrogen indicates that most of the NH_2 and OH groups react during the synthesis.

Furthermore, the optical absorption of C_3N_4 can be tuned by the addition of a small amount of BA to the complex. To make it more visible, FTO was picked as the model on which C_3N_4 films were deposited by copolymerization of CMp with 0, 5, and 15 mol % BA. The photograph in Figure 2a (bottom right) shows bare FTO and C_3N_4 films on FTO with different amounts of BA in the starting complex. The red shift of the C_3N_4 absorption with an increasing amount of BA (Figure S2c) was explained by Wang's group: the incorporation of BA affects the band structure of C_3N_4 by the replacement of nitrogen atoms with carbon.[24] SEM indicates that copolymerization with BA causes minor changes in the morphologies of the film (Figure S4). In principle, the strategy of supramolecular hydrogen-bonded complex chemistry allows the insertion of any desired molecule/element to the final C_3N_4 film, with the possibility to tune the optical and the electronic properties according to required applications.

The formation of a continuous and organized C_3N_4 layer on FTO was further confirmed by the strong photoluminescence (PL) of the modified C_3N_4. In general, changes in the electronic properties of organic semiconductors are reflected by their PL properties, which can be detected as evolution of the intensity or the shape of the recorded optical spectra. Figure 2b shows the PL spectra and a photograph of FTO/C_3N_4 films under UV illumination (365 nm). Similar to the absorption spectra, the emission peak of the C_3N_4 films is red-shifted with increasing amount of BA in the starting material. More interestingly, the C_3N_4 films exhibit high fluorescence quantum yields (QYs) (up to 0.17; Table S2) compared with the powder made from thermal condensation of the CM complex (QY ~ 0.01). The dramatic increase in QY indicates that the recombination of a higher fraction of C_3N_4 excitons in the C_3N_4 films occurs via radiative paths, presumably because of the continuity and reduced defects of C_3N_4 layers.

To support our view of a liquid-based C_3N_4 thin-film growth method, thermogravimetry (TG) and differential thermogravimetry (DTG) as well as a melting point apparatus (MPA) were employed to study the thermal properties of CMp. Figure 3a shows photographs of CMp powder in a capillary tube heated at controlled temperatures in the MPA, and the corresponding TG/DTG curves are shown in Figure 3b. The precursor did not undergo any mass loss until 252 °C, when it started to dehydrate, forming water on the inner surface of the capillary tube. The huge mass loss at 352 °C occurred at the same temperature as when the white powder turned to liquid, combined with bubbling from ammonia and phenyl group release.[16] To learn more about the relevant phase transformations, a control experiment was conducted in which the CMp precursor was heated to 365 °C (just above the fusing temperature) under nitrogen for 4 h and then cooled. The obtained powder showed the peak centered at 27.7° indicating the emergence of C_3N_4 along with small peaks from the original CMp complex (Figure 3c). Further increasing the temperature resulted in improved condensation of the CMp complex to C_3N_4, as will be shown below.

This intermediate state is considered the key step for the liquid-phase thin-film growth, which gives a strong advantage over its solid-phase counterpart: as opposed to loosely aggregated solid particles with gaps in between, different orientations, and poor contact with the substrate, the precursor

dx.doi.org/10.1021/ja508329c | J. Am. Chem. Soc. 2014, 136, 13486−13489

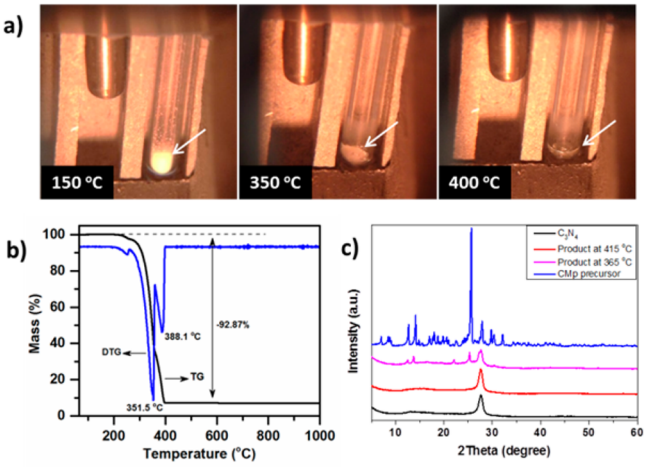

Figure 3. (a) State evolution of the CMp precursor in the melting point apparatus at controlled temperatures. (b) TG/DTG curves of the CMp complex in nitrogen. (c) XRD patterns of CMp, the thermal condensed products obtained at 365 and 415 °C, and final C_3N_4.

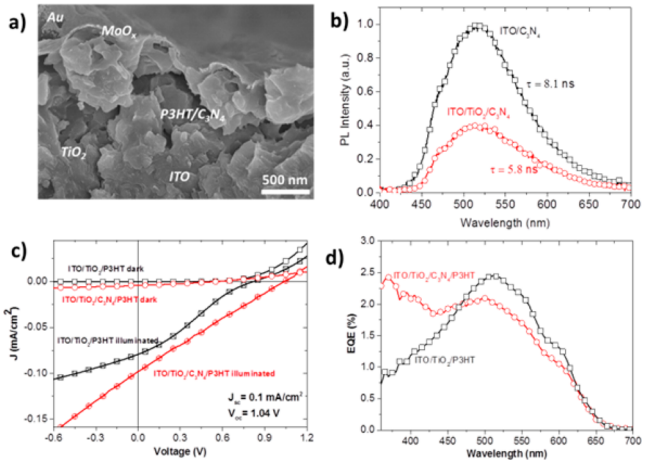

Figure 4. (a) Cross-sectional SEM image of a complete C_3N_4/P3HT solar cell. C_3N_4 and P3HT form an interpenetrated network. The TiO_2 and MoO_x layers are too thin to be resolved. (b) PL spectra and the corresponding fluorescence lifetimes of ITO/C_3N_4 and ITO/TiO_2/C_3N_4. (c) J–V curves for TiO_2/C_3N_4/P3HT and TiO_2/P3HT solar cells measured in darkness and under 100 mW/cm^2 AM 1.5G illumination. (d) EQEs of the cells under illumination.

in the liquid phase has a more intimate contact with the whole surface of the substrate, over which it can be distributed in a smooth, continuous manner. Besides, as we mentioned earlier, the morphology of porous networks of the C_3N_4 films is independent of the substrate, although the substrates possess completely different crystalline phases, surface morphologies, and roughnesses (Figure S5). Another dramatic mass loss was observed at 388 °C, which should be the result of further deamination. Figure 3a illustrates the transparent liquid at 400 °C, when the sample stopped showing any mass loss according to the TG curve. In this step, C_3N_4 already forms directly from the liquid phase during the heating process without going through any further intermediates, as shown in the XRD pattern (Figure 3c), while the final porous morphology observed via SEM arises from densification during rearrangements and improved organization, coupled with volume contraction within the final solid film. The porosity is highly beneficial for (photo)-electrochemistry applications, where more intimate contact with the second medium is eagerly requested, as for instance a liquid can infiltrate the electrode material.

It is worth noting that in order to confirm the critical role of the CMp complex for growth of C_3N_4 thin films, we also explored some other precursors that have been reported for C_3N_4 condensation, including dicyandiamide, melamine, and trithiocyanuic acid, to grow C_3N_4 films on FTO. In our experiments, none of these compounds led to uniform C_3N_4 films with well-defined thickness.

Replacing fullerene acceptors with polymers or metal oxides has been the subject of intense research,[25,26] but to date, fullerene-based organic solar cells remain the most efficient. Here we report a proof-of-concept device using C_3N_4 as the electron acceptor. The geometry (SEM) of the mesostructured heterojunction solar cell and the theoretical energy band diagram are illustrated in Figures 4a and S6, respectively. The cell consisted of a 40 nm TiO_2 layer on ITO as the electron transport layer and a C_3N_4 porous framework grown directly onto it as described above. Afterward, poly(3-hexylthiophene) (P3HT) was solution-cast onto the C_3N_4 to serve as both the electron donor and hole transporter. Partial infiltration of the porous carbon nitride network was achieved (Figure 4a, but there is still potential for improved infiltration as the C_3N_4 voids were not entirely filled with polymer. To enhance hole extraction, a 10 nm layer of molybdenum oxide was deposited onto the P3HT layer, followed by an 80 nm gold top electrode. As a reference, a solar cell without any C_3N_4 layer was also fabricated. Both devices (with or without C_3N_4) showed rectification behavior (Figure 4c), proving the formation of C_3N_4/P3HT and TiO_2/P3HT junctions. Under illumination, the C_3N_4/P3HT cell showed a surprisingly high open-circuit voltage (V_{oc}) of about 1 V, while the TiO_2/P3HT reference gave a maximum value of only 0.82 V. Furthermore, we note that the solar cell performance was almost unchanged for different pixel sizes between 0.5 and 16 mm^2. Despite the fact that the cell structure was not optimized, V_{oc} was higher than the best V_{oc} reported for TiO_2/P3HT (V_{oc} = 0.87 V for a mesoporous TiO_2/P3HT device)[25] and among the highest for polymer blends with P3HT as the electron donor.[26] We note that previous works on carbon nitride-like materials result in rather low V_{oc} and require vacuum deposition techniques for material preparation.[27,28]

The higher V_{oc} in devices containing carbon nitride may be explained by the fact that its presence reduces nonideality effects such as interfacial recombination of charges between TiO_2 and P3HT, trapping in TiO_2 defect states, and interfacial dipole formation upon charge transfer, all of which are known to lower V_{oc} in metal oxide:polymer solar cells.[29,30] In analogy to polymer:metal oxide and polymer:fullerene systems, Fermi level alignment upon the addition of C_3N_4 (Figure S6) can lead to higher V_{oc}, primarily limited by the offset between the P3HT HOMO and C_3N_4 LUMO. For the C_3N_4/P3HT cell, the contribution of C_3N_4 to the photocurrent was clearly shown in the shorter wavelength range (360–475 nm), while the onset of current generation was found at 650 nm and a peak value of ~2.4% was reached at 520 nm. Correspondingly, a short-circuit current density (J_{sc}) of 0.1 mA/cm^2 under simulated sunlight was obtained. Further evidence for charge separation at the C_3N_4/TiO_2 interface is given by the PL quenching and the fluorescence lifetime experiments (Figures 4b and S7). Our results show that in the presence of TiO_2, the C_3N_4 PL was quenched by 60% and the fluorescence lifetime shortened by 30%. These measurements confirm that under illumination most of the excited

dx.doi.org/10.1021/ja508329c | J. Am. Chem. Soc. 2014, 136, 13486–13489

electrons in C_3N_4 are transferred to the TiO_2. In order to further understand the role of C_3N_4, we fabricated cells with various layer thicknesses (Figures S8a and S9). The best performance was obtained for 500 nm thick C_3N_4. For thicker layers (>1 μm), both J_{sc} and V_{oc} dropped significantly (Figure S8b), potentially because of insufficient electron transport and a short exciton diffusion length due to enhanced recombination, while a thin C_3N_4 layer (~200 nm) was not uniform, resulting in shunts and thus low V_{oc}. In addition, we note that the thickness of the C_3N_4 may influence the P3HT/C_3N_4 interface and morphology, as the two parameters are closely linked as a result of the film formation process. Hence, the solar cell indeed demonstrates the potential of C_3N_4 as an electron acceptor, and further optimization of the polymer infiltration, surface modification, and layer thickness is likely to lead to a significant improvement in the photocurrent. Moreover, all of the mentioned adjustments should result in the improvement of the fill factor and consequently in the total cell efficiency. However, the high V_{oc}, simplicity, oxidation stability, and high availability are strongly encouraging for the fabrication of solar cells using C_3N_4 as an electron acceptor. The concept may also be particularly appealing to the field of meso-superstructured hybrid perovskite solar cells, as C_3N_4 can potentially serve as a stable organic mesostructured scaffold, replacing conventional metal oxides.

In summary, we have demonstrated a general method to grow C_3N_4 thin films on different substrates by liquid-mediated thermal condensation of a special precursor complex. The C_3N_4 films are continuous and show a homogeneous porous network structure regardless of the substrate. Moreover, the optical properties can easily be tuned in order to cover most of the visible spectrum. As an illustrative application of solution-processed carbon nitride in optoelectronics, we have demonstrated the integration of C_3N_4 into organic solar cells, reaching an open-circuit voltage of more than 1 V in combination with P3HT. We believe that this new deposition method will extend the opportunities for the fabrication of C_3N_4-based photoelectrochemical and optoelectronic devices. In addition, the high photoluminescence quantum yields and high thermal stability of C_3N_4 open new possibilities for C_3N_4-based electro- and photoluminescent devices.

■ ASSOCIATED CONTENT

Supporting Information

Experimental details and additional data. This material is available free of charge via the Internet at http://pubs.acs.org.

■ AUTHOR INFORMATION

Corresponding Authors

Menny.Shalom@mpikg.mpg.de
thbrenn@uni-potsdam.de

Notes

The authors declare no competing financial interest.

■ ACKNOWLEDGMENTS

M.S. is grateful for a Minerva Fellowship. T.J.K.B. thanks A. Kirch and T. Oliynyk for assistance with solar cell preparation, S. Reiter for AFM measurements, and the Helmholtz Energy Alliance ("Hybrid Photovoltaics") for financial support.

■ REFERENCES

(1) Thomas, A.; Fischer, A.; Goettmann, F.; Antonietti, M.; Müller, J.-O.; Schlögl, R.; Carlsson, J. M. *J. Mater. Chem.* **2008**, *18*, 4893.
(2) Zheng, Y.; Liu, J.; Liang, J.; Jaroniec, M.; Qiao, S. Z. *Energy Environ. Sci.* **2012**, *5*, 6717.
(3) Yan, S. C.; Li, Z. S.; Zou, Z. G. *Langmuir* **2009**, *25*, 10397.
(4) Lyth, S. M.; Nabae, Y.; Moriya, S.; Kuroki, S.; Kakimoto, M.-a.; Ozaki, J.-i.; Miyata, S. *J. Phys. Chem. C* **2009**, *113*, 20148.
(5) Yang, S.; Feng, X.; Wang, X.; Müllen, K. *Angew. Chem., Int. Ed.* **2011**, *50*, 5339.
(6) Zhu, J.; Carabineiro, S. A. C.; Shan, D.; Faria, J. L.; Zhu, Y.; Figueiredo, J. L. *J. Catal.* **2010**, *274*, 207.
(7) Yue, B.; Li, Q.; Iwai, H.; Kako, T.; Ye, J. *Sci. Technol. Adv. Mater.* **2011**, *12*, No. 034401.
(8) Zhang, Y.; Mori, T.; Ye, J.; Antonietti, M. *J. Am. Chem. Soc.* **2010**, *132*, 6294.
(9) Hong, J.; Xia, X.; Wang, Y.; Xu, R. *J. Mater. Chem.* **2012**, *22*, 15006.
(10) Maeda, K.; Wang, X.; Nishihara, Y.; Lu, D.; Antonietti, M.; Domen, K. *J. Phys. Chem. C* **2009**, *113*, 4940.
(11) Liang, J.; Zheng, Y.; Chen, J.; Liu, J.; Hulicova-Jurcakova, D.; Jaroniec, M.; Qiao, S. Z. *Angew. Chem., Int. Ed.* **2012**, *51*, 3892.
(12) Kailasam, K.; Epping, J. D.; Thomas, A.; Losse, S.; Junge, H. *Energy Environ. Sci.* **2011**, *4*, 4668.
(13) Cao, S.-W.; Liu, X.-F.; Yuan, Y.-P.; Zhang, Z.-Y.; Liao, Y.-S.; Fang, J.; Loo, S. C. J.; Sum, T. C.; Xue, C. *Appl. Catal., B* **2014**, *147*, 940.
(14) Zhang, Y.; Mori, T.; Ye, J. *Energy Environ. Sci.* **2011**, *4*, 4517.
(15) Jun, Y. S.; Lee, E. Z.; Wang, X.; Hong, W. H.; Stucky, G. D.; Thomas, A. *Adv. Funct. Mater.* **2013**, *23*, 3661.
(16) Ishida, Y.; Chabanne, L.; Antonietti, M.; Shalom, M. *Langmuir* **2014**, *30*, 447.
(17) Zhang, J.; Zhang, G.; Chen, X.; Lin, S.; Möhlmann, L.; Dołęga, G.; Lipner, G.; Antonietti, M.; Blechert, S.; Wang, X. *Angew. Chem., Int. Ed.* **2012**, *51*, 3183.
(18) Zhang, Y.; Mori, T.; Ye, J. *Sci. Adv. Mater.* **2012**, *4*, 282.
(19) Yang, F.; Lublow, M.; Orthmann, S.; Merschjann, C.; Tyborski, T.; Rusu, M.; Kubala, S.; Thomas, A.; Arrigo, R.; Hävecker, M.; Schedel-Niedrig, T. *ChemSusChem* **2012**, *5*, 1227.
(20) Zheng, Y.; Jiao, Y.; Chen, J.; Liu, J.; Liang, J.; Du, A.; Zhang, W.; Zhu, Z.; Smith, S. C.; Jaroniec, M.; Lu, G. Q.; Qiao, S. Z. *J. Am. Chem. Soc.* **2011**, *133*, 20116.
(21) Yang, S.; Feng, X.; Wang, X.; Müllen, K. *Angew. Chem., Int. Ed.* **2011**, *123*, 5451.
(22) Shalom, M.; Gimenez, S.; Schipper, F.; Herraiz-Cardona, I.; Bisquert, J.; Antonietti, M. *Angew. Chem., Int. Ed.* **2014**, *53*, 3654.
(23) Holst, J. R.; Gillan, E. G. *J. Am. Chem. Soc.* **2008**, *130*, 7373.
(24) Zhang, J. S.; Chen, X. F.; Takanabe, K.; Maeda, K.; Domen, K.; Epping, J. D.; Fu, X. Z.; Antonietti, M.; Wang, X. C. *Angew. Chem., Int. Ed.* **2010**, *49*, 441.
(25) Wright, M.; Uddin, A. *Sol. Energy Mater. Sol. Cells* **2012**, *107*, 87.
(26) Vaynzof, Y.; Kabra, D.; Brenner, T. J. K.; Sirringhaus, H.; Friend, R. H. *Isr. J. Chem.* **2012**, *52*, 496.
(27) Zhou, Z. B.; Cui, R. Q.; Pang, Q. J.; Hadi, G. M.; Ding, Z. M.; Li, W. Y. *Sol. Energy Mater. Sol. Cells* **2002**, *70*, 487.
(28) Byers, J. C.; Billon, F.; Debiemme-Chouvy, C.; Deslouis, C.; Pailleret, A.; Semenikhin, O. A. *ACS Appl. Mater. Interfaces* **2012**, *4*, 4579.
(29) Noori, K.; Giustino, F. *Adv. Funct. Mater.* **2012**, *22*, 5089.
(30) Blakesley, J. C.; Neher, D. *Phys. Rev. B* **2011**, *84*, No. 075210.